Hindawi
Shock and Vibration
Volume 2022, Article ID 6397602, 14 pages
https://doi.org/10.1155/2022/6397602

Research Article

Development of a Negative Stiffness Bistable Damper for Structural Vibration Control

Liming Fan, Chen Huang, and Linsheng Huo

State Key Laboratory of Coastal and Offshore Engineering, Dalian University of Technology, Dalian 116023, China

Correspondence should be addressed to Linsheng Huo; lshuo@dlut.edu.cn

Received 5 August 2022; Revised 12 October 2022; Accepted 21 October 2022; Published 1 November 2022

Academic Editor: Salvatore Caddemi

Linear dampers have been widely applied for suppressing the dynamic responses of structures to mitigate their damage. However, the primary disadvantage of the classical linear damper is that it is vulnerable to detuning, which has become an issue of great importance recently due to a great reduction in vibration control performance. To overcome the shortcoming, this study develops a negative stiffness bistable damper (NSBD) composed of a simple assembly consisting of a bistable buckling beam with a mass. Energy is dissipated through the transformation between the bistable states. The constitutive equation of the NSBD is derived to analyze the effects of the stiffness ratio, the arch-span ratio, and the damping ratio on its restoring capabilities. The vibration reduction effect of the NSBD is experimentally evaluated under different sinusoidal and seismic excitations in shaking table tests. The obtained results reveal that the NSBD can effectively restrain structural displacements.

1. Introduction

Vibration control is well-established since first proposed by Yao [1] in 1972, yet still developed to enhance the functionality and safety of structures. Up to now, many structures have been installed with various types of vibration control devices to restrain their responses to wind loads, seismic action, or other dynamic excitations [2–5]. Linear dampers (e.g., tuned mass damper) have been widely applied in engineering practice, such as the vibration control systems of the Akashi Kaikyo Bridge [6], the Taipei 101 tower [7], and the Shanghai Center Tower [8].

Generally, the dynamic response of a structure is greatly influenced by the first frequency and vibration mode [9–11]. The conventional tuned mass damper (TMD) must keep consistent with the first frequency of the primary structure to effectively restrain the structural vibration. Therefore, as a type of frequency-sensitive device, the conventional TMD operates within a relatively narrow frequency band for vibration reduction. The TMD is detuned and its effectiveness can be evidently reduced when the natural frequency of the host structure alters.

To overcome this deficiency, many negative stiffness vibration control devices have been developed. The concept of negative stiffness was first introduced by Molyneaux [12]. When the directions of restoring force and corresponding deformation are opposite, their ratio is negative. A structure in such a state has negative stiffness. For structural vibration control, the negative stiffness can reduce the stiffness of the control system and thus lower its natural frequency, allowing it to provide vibration reduction over a wide frequency range. Negative stiffness can be achieved via various methods. Traditionally, negative stiffness is achieved by special mechanical devices for energy storage elements (e.g., spring and prebuckled beam) [13–17], magnetic elements [18–20], geometric nonlinearities [21–23], or composite structures and metamaterials [23, 24]. Virgin et al. [25] proposed negative vibration isolation using a highly deformed, slender beam. The isolator had a high adjustable stiffness and a high rate of displacement transmission over a wide range. Shi and Zhu [26] developed and experimentally verified two configurations of magnetic negative stiffness dampers (MNSDs), in which multiple permanent magnets are placed in a conductive tube. Zhou et al. [27]. introduced a negative stiffness vibration isolation damper (NSVID) using

a nonlinear structure and utilized the NSVID to control torsional vibration along a shaft. This proposed device can realize quasi-zero stiffness (QZS) by changing the stiffness of rubber and control parameters. Xiang et al. [28] designed a semiactive control torsional vibration damper, which is composed of positive and negative stiffness in parallel. They provided a derivation of the theory behind the damper mechanism and analyzed its elastic properties. Zhou et al. [29] conducted theoretical analysis and experimental studies on a passive negative stiffness damper (PNSD) in series with flexible support. The results indicated that their proposed device can achieve a range of equivalent negative stiffnesses and Coulomb values. Haghpanah et al. [24] invented a negative stiffness element composed of one convex elastic element together with elastic elements that have nonconvex strain energy. This element can greatly enhance damping performance under dynamic excitation. Recently, numerous other negative stiffness dampers have been introduced for vibration control of various types of excitations [30–34] and different types of structures [35–37].

Bistable structures are structures that not only have negative stiffness properties, but can also provide cubic stiffness to enhance vibration control. Most previous studies focused on mechanical properties analysis [38, 39] and vibration isolation applications of bistable structures. Johnson et al. [40] studied the vibration-attenuating effect of a bistable oscillator and investigated its snap-through dynamics using the harmonic balance method and experimentation. Experimental results show that the bistable oscillator has a slightly superior vibration attenuation performance compared to the fundamental harmonic snap-through action. Farhangdoust et al. [41]. introduced a bistable tuned mass damper (BTMD) mechanism for suppressing the vortex-induced vibration (VIV) in suspension bridge decks, which are exceptionally sensitive to broadband input of vortex shedding velocity. Xia et al. [42] investigated the enhancement in vibration attenuation bandwidth of a locally resonant metamaterial beam with bistable attachments, the interwell oscillations of the attachments produced an attenuation frequency range of 350% wider than linear locally resonant bandgap for moderate-to-high amplitude excitation levels. Zhao et al. [43] explored multiple snap-through pathways and force-displacement curves of a discontinuous point and verified the results through theoretical analysis and numerical simulation. Liu et al. [44] used equivalent, analytical, numerical, and experimental methods to investigate 1/2 sub-harmonic resonance in a bistable structure and its vibration isolation characteristics. Zhang et al. [45] designed a recoverable inclined beam energy absorption structure that leverages bistable characteristics to improve the safety and efficiency of passive energy absorption systems in automobiles. Yan et al. [46, 47] invented a bistable vibration isolation (BVI) device composed of several ring permanent magnets (PMS). The PMS improved the vibration isolation performance of the BVI through nonlinear electromagnetic shunt damping. Zhang et al. [48] utilized an optimized and varying sectional profile to improve the performance of a quasi-zero stiffness (QZS) isolation system using the nonlinear and negative stiffness generated by the snap-through effect of bistable structures. Yang et al. [49] proposed a feedback control law to modulate the current input to the actuator of an active vibration isolation system. The proposed control law greatly attenuated the transmissibility of the bistable nonlinear electromagnetic actuator from the base excitation.

Inspired by the advantages of negative stiffness and bistable structures, this paper proposes a negative stiffness bistable damper (NSBD) composed of a bistable buckling beam assembled with a mass. The NSBD can enhance energy dissipation through the transformation between the bistable states. The key component of the damper is a precompressed spring steel set in a clamped-clamped configuration in the frame structure. The constitutive equation of the NSBD is derived to analyze the effects of the stiffness ratio, the arch-span ratio, and the damping ratio on the restoring force of the NSBD. To validate the vibration reduction effect of the NSBD, a frame structure was subjected to shake table tests with and without the NSBD. Finally, a following discussion of the experimental results is presented to explore the damping effect of different parameters on the NSBD.

2. Constitutive Equation of Negative Stiffness Bistable Damper

2.1. Mechanical Characterization of Negative Stiffness Bistable Damper. A schematic of a linear single-degree-of-freedom (SDOF) structure equipped with an NSBD is depicted in Figure 1. The mass, stiffness, and damping coefficient of the structure are m_1, k_1, and c_1, respectively. In the schematic, k_{ns} is the stiffness of the NSBD and consists of the negative stiffness k_{21} and the cubic stiffness k_{22}. The key component of the NSBD is the bistable buckling beam, which is clamped within the frame structure and precompressed. An attached mass is fixed at the midspan of the bistable buckling beam. When an external excitation acts on the primary structure, the NSBD will be continuously transformed between two equilibrium positions.

Under small transverse displacement, the prestress imposed along the axial direction (y direction) of the straight beam to move the right end of the beam from position b to position a results in displacement w_y in the y direction. The prestress also causes the force P to be applied in the x-direction at the midpoint of the beam, resulting in displacement w_x in the x-direction, as shown in Figure 2. The deflection curve of the deformed beam is the first-order mode shape of the clamped-clamped beam.

$$w(\mathrm{y}) = \frac{w_x}{2}\left[1 - \cos\left(\frac{2\pi y}{l_c}\right)\right]. \tag{1}$$

Assuming that the beam section thickness is δ and the beam section width is b, the moment of inertia and cross-sectional area of the beam section are, respectively, $I = (b\delta^3/12)$ and $A = b\delta$. The axial stiffness of the beam is $k_0 = (AE/l_c)$. According to Jin et al. [50], the relationship between the external force on the buckling beam and the displacement is as follows:

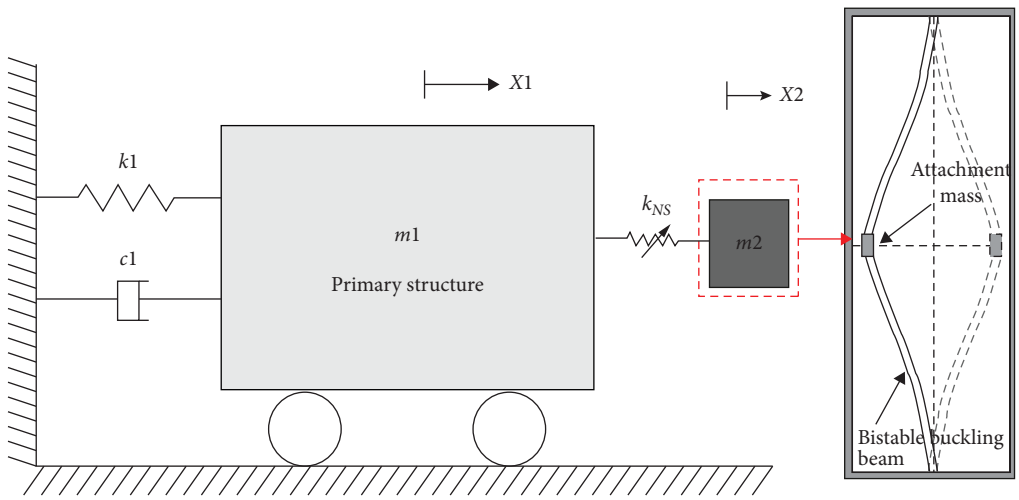

Figure 1: Schematic diagram of NSBD.

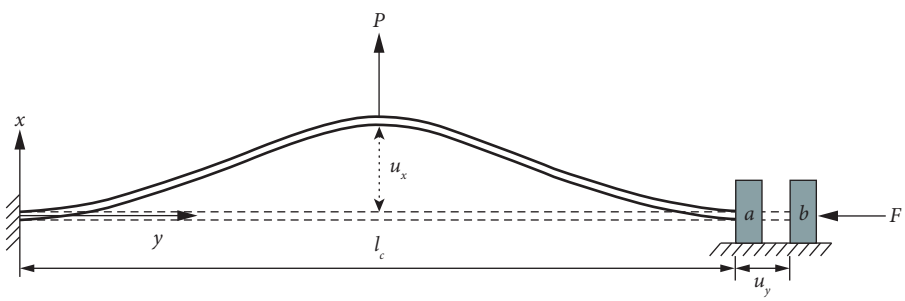

Figure 2: The buckled beam with prestress.

$$F_0 = \left(\frac{3\pi^4 Q^2}{2}\right)\Delta\left[\Delta - \frac{3}{2} - \sqrt{\frac{1}{4} - \frac{4}{3Q^2}}\right] \times \left[\Delta - \frac{3}{2} + \sqrt{\frac{1}{4} - \frac{4}{3Q^2}}\right], \tag{2}$$

where $F_0 = (pl_c^3/EI\delta)$, $\Delta = (\sigma/\delta)$, and $Q = (w_y/\delta)$ are normalized parameters. l_c is the span of the buckling beam and δ is the thickness. σ is the intermediate deformation of the buckling beam under external force, and w_y is the arching height of the buckling beam.

The model parameters of the bistable buckling beam are solved by equation (2) and transformed into the ordinary form:

$$\begin{aligned}\frac{Pl_c^3}{EIw_y} &= \frac{3\pi^4}{2}\left(\frac{w_y}{\delta}\right)^2\left(\frac{\sigma}{w_y}\right)^3 - \frac{9\pi^4}{2}\left(\frac{w_y}{\delta}\right)^2\left(\frac{\sigma}{w_y}\right)^2 \\ &\quad + \left[3\pi^4\left(\frac{w_y}{\delta}\right)^2 + 2\pi^4\right]\left(\frac{\sigma}{w_y}\right),\end{aligned} \tag{3}$$

$$P = \frac{3\pi^4 EI}{2l_c^3\delta^2}\sigma^3 - \frac{9\pi^4 EIw_y}{2l_c^3\delta^2}\sigma^2 + \left(\frac{3\pi^4 w_y^2 EI}{\delta^2 l_c^3} + \frac{2\pi^4 EI}{l_c^3}\right)\sigma. \tag{4}$$

The formula (5) can be obtained by placing the zero position at the origin.

$$\begin{aligned}P &= \frac{3\pi^4 EI}{2l_c^3\delta^2}(x+\sigma)^3 - \frac{9\pi^4 EIw_y}{2l_c^3\delta^2}(x+\sigma)^2 + \left(\frac{3\pi^4 w_y^2 EI}{\delta^2 l_c^3} + \frac{2\pi^4 EI}{l_c^3}\right)(x+\sigma) \\ &= \frac{3\pi^4 EI}{2l_c^3\delta^2}x^3 - \left(\frac{3\pi^4 w_y^2 EI}{2\delta^2 l_c^3} - \frac{2\pi^4 EI}{l_c^3}\right)x + \frac{2\pi^4 EIw_y}{l_c^3}.\end{aligned} \tag{5}$$

Thus, the cubic stiffness coefficient of the buckling beam can be expressed as $(3\pi^4 EI/2l_c^3\delta^2)$, The negative stiffness coefficient of the buckling beam is $-((3\pi^4 EI/2\delta^2 l_c^3) - (2\pi^4 EI/l_c^3))$. When $E = 198.6$ GPa, $l_c = 0.36$ m, $\delta = 0.0002$ m, $w_y = 0.025$ m, and $b = 0.02$ m, the relationship between force and displacement of the buckling beam is shown in Figure 3.

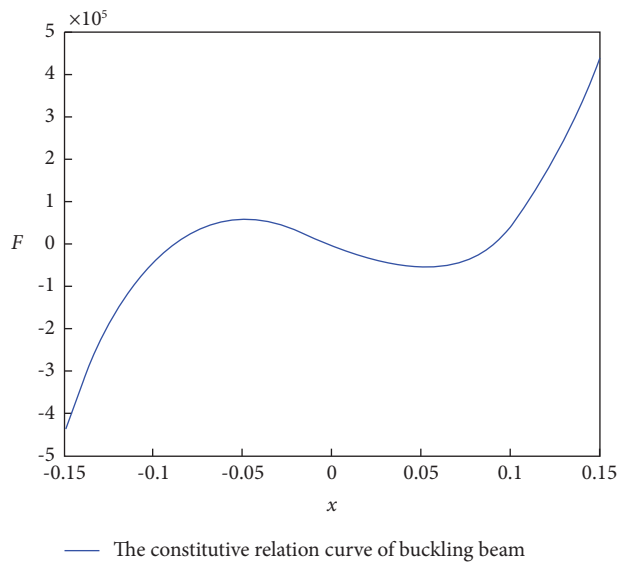

Figure 3: Force and displacement curve of buckling beam.

2.2. Stiffness Analysis. From the above analysis, it can be seen that the stiffness expression of the buckling beam is as follows:

$$\begin{aligned} k &= \frac{\partial P}{\partial x} \\ &= \frac{3\pi^4 EI}{2l_c^3\delta^2}x^2 - \left(\frac{3\pi^4 w_y^2 EI}{2\delta^2 l_c^3} - \frac{2\pi^4 EI}{l_c^3}\right) \\ &= \frac{3\pi^4 EI}{2l_c^3}\left[\frac{x^2}{\delta^2} - \frac{w_y^2}{\delta^2} + \frac{4}{3}\right]. \end{aligned} \tag{6}$$

The axial stiffness of the buckling beam is

$$k_0 = \frac{AE}{l_c}. \tag{7}$$

Then, the equivalent stiffness of the buckling beam is

$$\overline{k} = \frac{k}{k_0} = \frac{\pi^4}{8}\left[\overline{x}^2 - \phi^2 + \frac{4}{3}\eta^2\right], \tag{8}$$

where $\overline{k} = (k/k_0)$, $\eta = (\delta/l_c)$, $\phi = (w_y/l_c)$, $\overline{x} = (x/l_c)$.

The variation of equivalent stiffness of buckling beam with different camber heights is shown in Figure 4.

3. Parametric Analysis

3.1. Mechanical Constitutive Equation of Buckling Beam. From the above derivation, it can be seen that the mechanical constitutive equation of the buckling beam can be composed of a negative stiffness term and a cubic nonlinear term as follows:

$$F = -k_{21}x + k_{22}x^3, \tag{9}$$

where k_{21} and k_{22} are, respectively, the negative stiffness coefficient and cubic stiffness coefficient. Therefore, the potential energy function of the buckling beam is as follows:

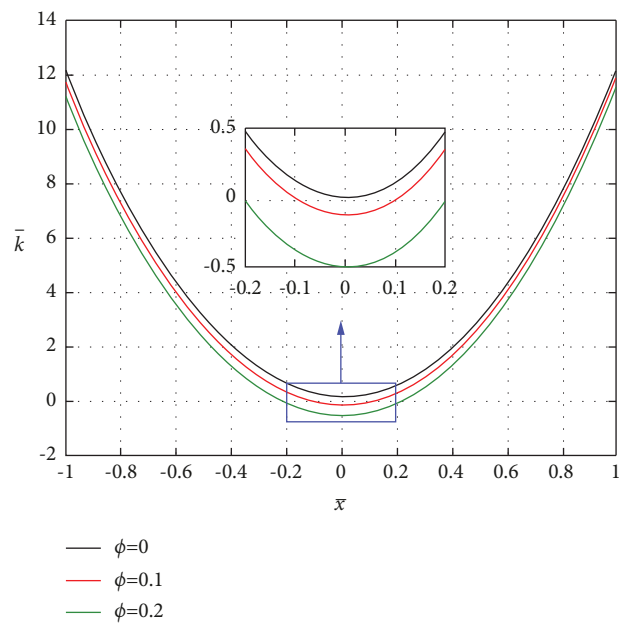

Figure 4: Relationship between equivalent stiffness of buckling beam and camber height.

$$U(x) = -\frac{1}{2}k_{21}x^2 + \frac{1}{4}k_{22}x^4. \tag{10}$$

Letting $F = 0$, the equilibrium position of the buckling beam can be obtained as shown in equation (11).

$$x_0 = \pm\sqrt{\frac{k_{21}}{k_{22}}}. \tag{11}$$

Although the stiffness of the buckling beam changes with a change in position during vibration, the response characteristics are approximately linear when the buckling beam vibrates at the equilibrium point with a very small amplitude. Therefore, the stiffness of the buckling beam is simplified with the linear stiffness at the equilibrium position in the parametric analysis. In the analysis, the equivalent stiffness is used for simplification. The equivalent stiffness is as follows:

$$k_e = \frac{d^2U(x)}{dx^2} = \left(-k_{21} + 3k_{22}x^2\right)\big|_{x=x_0} = 2k_{21}. \tag{12}$$

The equivalent frequency of the buckled beam is

$$\omega_e = \sqrt{\frac{k_e}{m}}. \tag{13}$$

From the potential energy function of the buckling beam, the bistable limit position can be solved as

$$U(x) = -\frac{1}{2}k_{21}x^2 + \frac{1}{4}k_{22}x^4 = 0, \tag{14a}$$

$$x_{cr} = \pm\sqrt{\frac{2k_{21}}{k_{22}}} = \frac{|x_0|}{\sqrt{2}}. \tag{14b}$$

It can be seen that when the applied external load meets the condition $A_0 > x_{cr}$, the buckling beam is in bistable vibration, and when $A_0 \leq x_{cr}$, the buckling beam experiencing monostable vibration.

3.2. Analytical Derivation. When the buckling beam with fixed ends is subjected to sinusoidal excitation with amplitude F and frequency ω, the beam can be simplified into an SDOF system. The dynamic equation of the buckled beam is as follows:

$$m\ddot{x} + c\dot{x} - k_{21}x + k_{22}x^3 = F\sin(\omega t), \tag{15}$$

where m, c,and k_{21}, k_{22} refer to the mass, damping, and negative stiffness and cubic stiffness of the buckling beam, respectively; the equation (16) can be simplified to

$$\ddot{y} + 2\xi\dot{y} - y + \alpha f^2 y^3 = \sin(\theta\tau), \tag{16}$$

where $\xi = (c/2m\omega)$, $\alpha = (k_{22}/k_{21})$, $\omega_1 = \sqrt{(k_{21}/m)}$, $\theta = (\omega/\omega_1)$, $y = (x/f)$, $f = (F/k_{22})$, and $\tau = \theta t$.

In order to obtain an approximate solution, the harmonic balance method is adopted in the paper, as used to solve equation (16); the first-order approximate solution is assumed to be as follows:

$$y = Y\sin(\theta\tau + \varphi). \tag{17}$$

In the analysis, the first-order approximate solution is considered, by substituting equation (17) into equation (16), and approximating $\sin^3\theta = (3/4)\sin\theta - (1/4)\sin 3\theta \approx (3/4)\sin\theta$, the following relationships are obtained:

$$-\theta^2 Y - Y + \alpha f^2 \times \frac{3}{4}Y^3 = \cos\varphi, \tag{18a}$$

$$2\xi\theta Y = -\sin\varphi. \tag{18b}$$

By combined equations (18a) and (18b) and eliminating φ, equation (19) can be obtained as follows:

$$\frac{9}{16}\alpha^2 f^4 Y^6 - \frac{3}{2}\alpha f^2 Y^4\left(1+\theta^2\right) + \left(4\xi^2\theta^2 + \theta^4 + 2\theta^2 + 1\right)Y^2 - 1 = 0. \tag{19}$$

Rearranging equation (19) to be expressed in terms of θ is

$$Y^2\theta^4 + \left(4\xi^2 Y^2 - \frac{3}{2}\alpha f^2 Y^4 + 2Y^2\right)\theta^2 + \left(\frac{9}{16}\alpha^2 f^4 Y^6 - \frac{3}{2}\alpha f^2 Y^4 + Y^2 - 1\right) = 0. \tag{20}$$

The solution of the equation is thus

$$\theta = \sqrt{\left(\frac{3}{4}\alpha f^2 Y^2 - 2\xi^2 - 1\right) \pm \sqrt{4\xi^4 + 4\xi^2 - 3\alpha\xi^2 f^2 Y^2 + \frac{1}{Y^2}}}. \tag{21}$$

The amplitude-frequency response function of the buckled beam can be obtained by solving equation (21), as shown in Figure 5.

The amplitude-frequency response curve of a linear system is constant; however, the amplitude-frequency response curve of the nonlinear system depends on the initial value conditions. Figure 5 reveals the relation between the amplitude of the response of the nonlinear system and the excitation frequency at the following initial conditions: (a) $\xi = 0.03$, $\alpha = 0.3$, (b) $\xi = 0.03$, $f = 0.5$, and (c) $f = 0.5$, $\alpha = 0.3$. It can be noted that the negative stiffness term and the nonlinear term make the curve bend towards the right, resulting in one frequency value corresponding to multiple amplitudes in the frequency range.

Figure 5(a) shows the relationship between the amplitude of the system ($\xi = 0.03$, $\alpha = 0.3$) response at different f and the excitation frequency. As the nonlinear coefficient increases, the maximum amplitude of the response decreases, but the degree of curvature does not change. The upward jump point is also getting smaller.

Figure 5(b) shows the relationship between the amplitude response of the nonlinear system ($\xi = 0.03$, $f = 0.5$) at different ∂ and the excitation frequency. Note that as the nonlinear coefficient increases, the bend of the curve does not change appreciably, but the upward jump point also decreases.

Figure 5(c) shows the relationship between the amplitude of the system response ($f = 0.5$, $\alpha = 0.3$) with different damping ratio ξ and the excitation frequency. With the increase of the damping ratio, the bending degree of the curve does not change, and the upward jump point is also unchanged.

4. Experiment Setup and Conditions

4.1. Experiment Setup. Based on the above discussion, experiments are designed to verify the attenuating effect of NSBD on the vibration response of frame structure and study the influence of the relevant parameters on the vibration response of frame structure. The main component of the damper is a buckling beam made of spring steel, which can reach different camber heights depending on an external force. The clamped-clamped buckling beam is fixed within a steel frame supported by four circular steel columns. To better enable the bistable effect, the attached mass is added to the midspan of the buckling beam. The whole experimental device is fastened on the shaking table using bolts. Under the transverse acceleration provided by the shaking table, the mass block is used to provide the driving force according to $F = ma$ to cause the device to switch between the two equilibrium positions and thus provide vibration reduction. The experimental device is shown in Figure 6. The experiments are conducted with and without the NSBD coupled with the frame structure.

A data acquisition system is (DH5922D dynamic signal test and analysis system) connected to a computer recorded data from a laser displacement sensor that measures the movements of the frame. The setup of the experiment and instrumentation is shown in Figure 6. As shown in Figure 6, before installing the NSBD system, holes are reserved in the center of the beam and the square frame, respectively. In the experiment, the

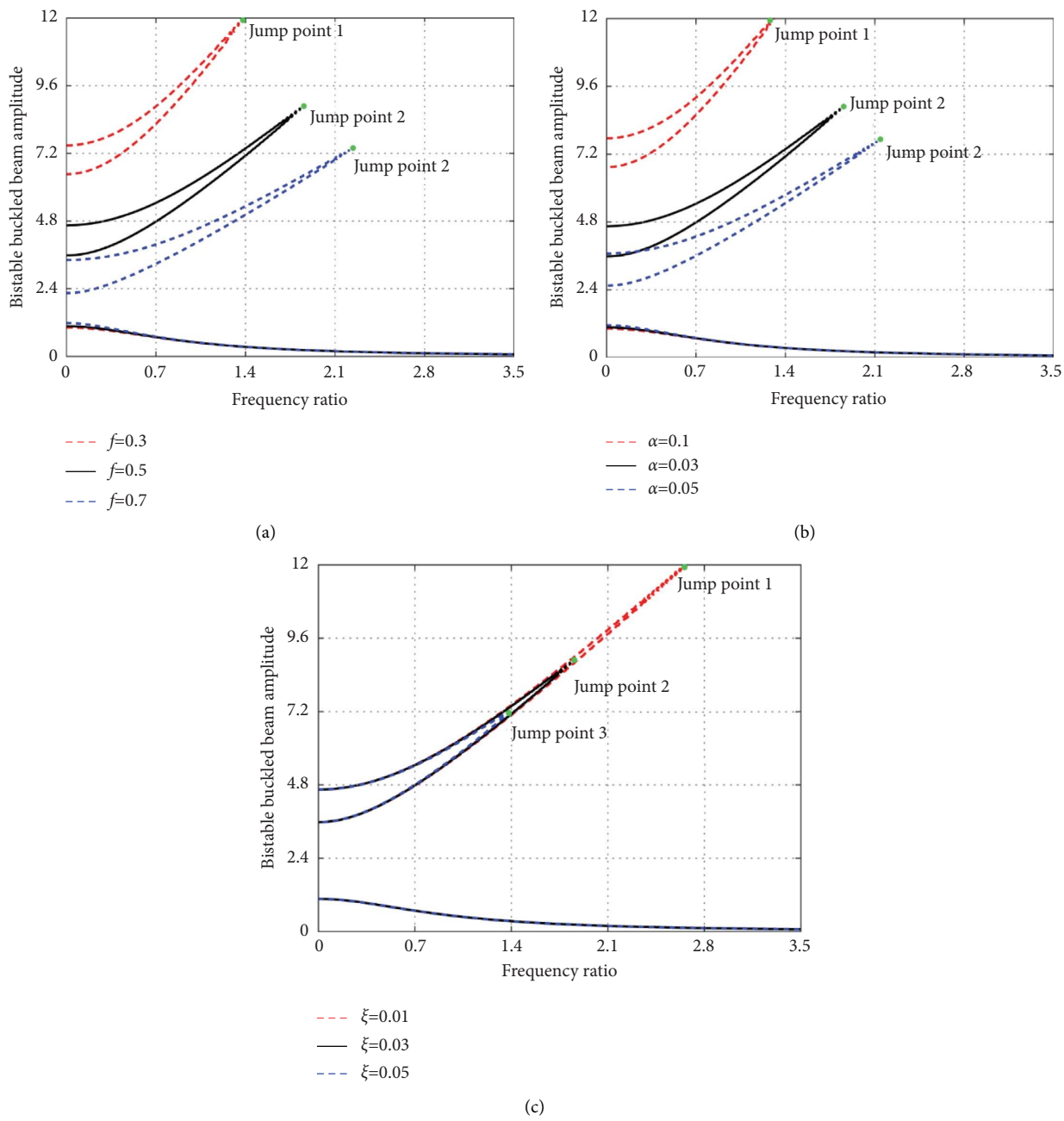

Figure 5: The amplitude-frequency response curve of the buckled beam.

buckling beam is guided freely through the clamping parts of the square frame at both ends. Then, prepressure is applied to both ends of the buckling beam to make the buckling beam reach the specified height, and the corresponding mass blocks are bolted in the middle of the buckling beam according to the experimental requirements after the two ends of the buckling beam are fixed; then the NSBD system is completed.

The buckling beam in the experiment is arched using spring steel with a prepress at the end, and a mass composed of a square iron block is fixed in the middle of the span. The mass of the block can be changed to adjust the characteristics of the NSBD. In the experiment, the spring steel is restrained by a square steel tube to control the height of the buckling beam arch. The support system of the frame structure consisted of four round steel columns that are fixed on the shaking table with bolts. The experimental parameters are listed in Table 1.

4.2. Experimental Conditions. In the experiment, the effects of the arch-span ratio (i.e., the ratio of arch height to the buckling beam span) and the mass ratio (i.e., the ratio of additional mass block mass to the frame mass) on the vibration reduction performance of NSBD are considered. The arch-span ratio and mass used in the experiment are listed in Tables 2 and 3.

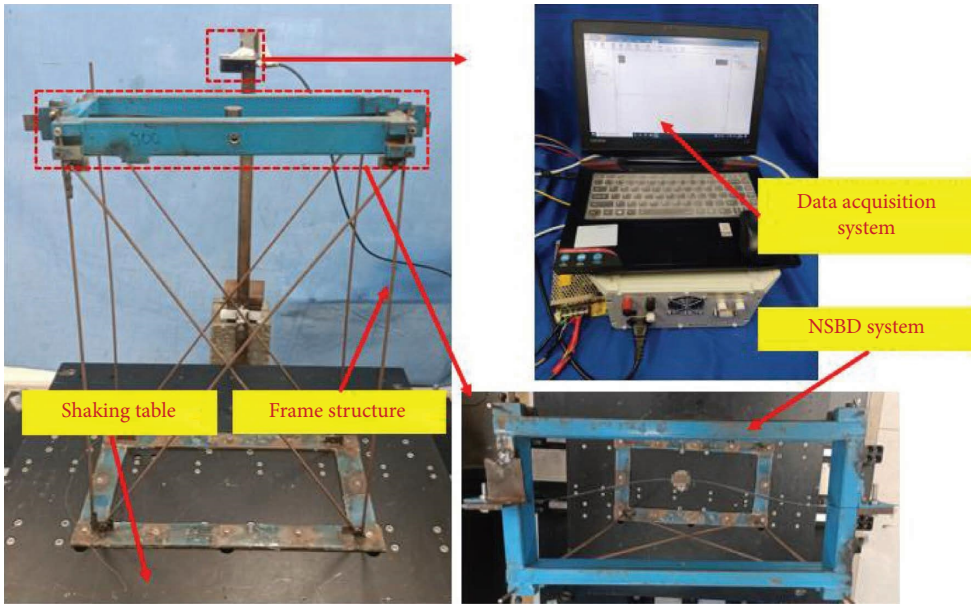

Figure 6: Experimental device.

Table 1: Experimental parameters.

Experimental materials	Parameter value	
	A	*B*
Frame size	20 mm × 40 mm × 150 mm	20 mm × 40 mm × 400 mm
Buckling beam thickness	0.2 mm	0.25 mm
Mass of mass block	69.26 g	111.6 g
Buckling beam width	20 mm	
Buckling beam density	7.85 g/cm^3	
Buckling beam elastic modulus	198.6 N/mm^3	
Support system	Ø4mm × 600 mm	

Table 2: Arch-span ratio.

Arch height (mm)	Beam span (mm)	Ratio (%)
15		0.42
25	3600	0.69
35		0.97

Table 3: Mass ratio.

Attachment mass (g)	Mass of primary structure (g)	Ratio (%)
69.26	5050	1.37
111.6		2.21

The experiment validated the attenuating effect of NSBD on the frame structure under sinusoidal and earthquake excitation. Firstly, the shaking table is used to perform a frequency sweep analysis of the experimental frame structure. The analysis determined that the natural frequency of the experimental frame structure is 2.89 Hz. Based on the switch threshold force of the buckling beams for different thicknesses, the amplitude of sinusoidal excitation applied to the frame structure is 0.05 cm. Secondly, the experiments used sinusoidal excitations to examine the damping provided by the NSBD for frame structures of different thicknesses. Finally, a total of 10 different earthquake excitations selected from two types of sites are used to investigate the vibration control effectiveness of the NSBD at the best damping. According to the code (GB5011-2010) [51], 10 different earthquake excitations are selected, as listed in Table 4, which represent different site conditions.

5. Experiment Results

5.1. Vibration Control Effectiveness under Sinusoidal Excitation. Sweep sine excitations (0.05 displacement) ranged between 2.78 Hz and 3.0 Hz at 0.1 Hz intervals are used to test the effectiveness of the NSBD at and near the natural frequency. The frequency-displacement responses of the frame structure for the different configurations of the NSBD are shown in Figure 7 and the corresponding time history responses are shown in Figure 8.

As shown in Figure 7, the inclusion of the NSBD reduced the vibrations of the frame structure especially for those under $\delta = 0.2$ mm, $\mu = 2.21\%$, and $h = 35$ mm. The installation of the NSBD shifted the natural frequency far away from the dominant excitation frequency, thus providing a great damping effect between 2.86 Hz and 3.0 Hz. The vibration of frame structure can therefore be suppressed effectively by

Table 4: Information of the selected seismic records.

Site classification	Earthquake name	Year	Station	Magnitude	R_{rup} (km)	V_{s30} (m/s)
I	Imperial Valley-03	1951	EI Centro Array #9	5.6	25.24	213.44
	Southern Calif	1952	San Luis Obispo	6	73.41	493.5
	Imperial Valley-05	1955	El Centro Array #9	5.4	14.88	213.44
	Central Calif-02	1960	Hollister City Hall	5	9.02	198.77
	Hollister-01	1961	Hollister City Hall	5.6	19.56	198.77
	San Fernando	1971	Pasadena - Old seismo lab	6.61	21.5	969.07
II	Guy_2010-10-15-HHE	2010	X102 Temporary Station_ Greenbriar_ AR	3.86	12.26	495.3
	Guy_2010-10-15-HHN	2010	X102 Temporary Station_ greenbriar_ AR	3.86	12.26	495.3
	Mineral_2011-08-23	2011	Keystone College_ La Plume_ PA	5.74	442.73	689.9
	Sparks_2011-11-05	2011	Smith Ranch_ Marlow_ OK	4.73	148.55	548.4

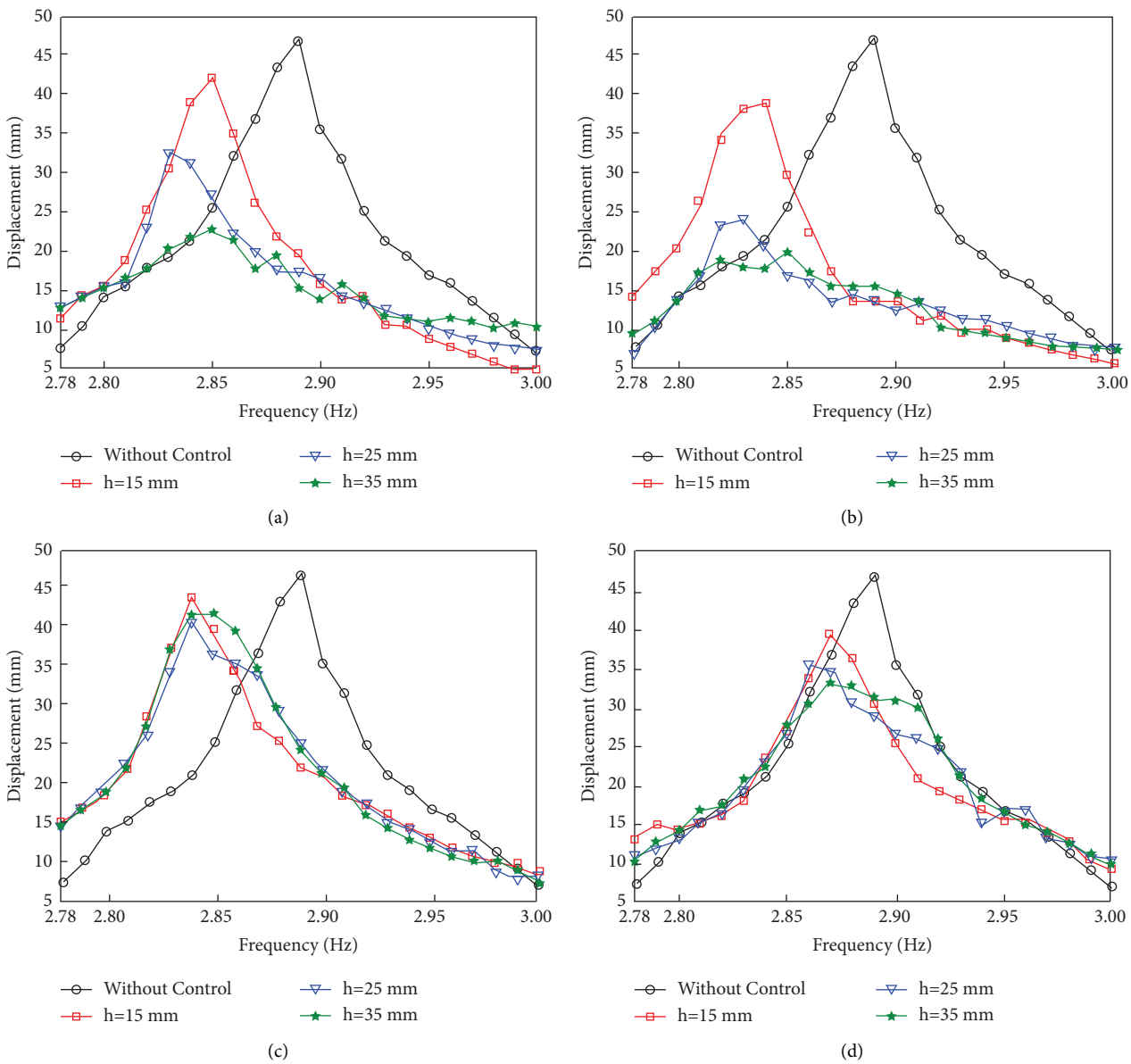

Figure 7: Frequency-displacement response of frame structure with different parameters: (a) $\delta = 0.2$ mm, $\mu = 1.37\%$, (b) $\delta = 0.2$ mm, $\mu = 2.21\%$, (c) $\delta = 0.25$ mm, $\mu = 1.37\%$, and (d) $\delta = 0.25$ mm, $\mu = 2.21\%$.

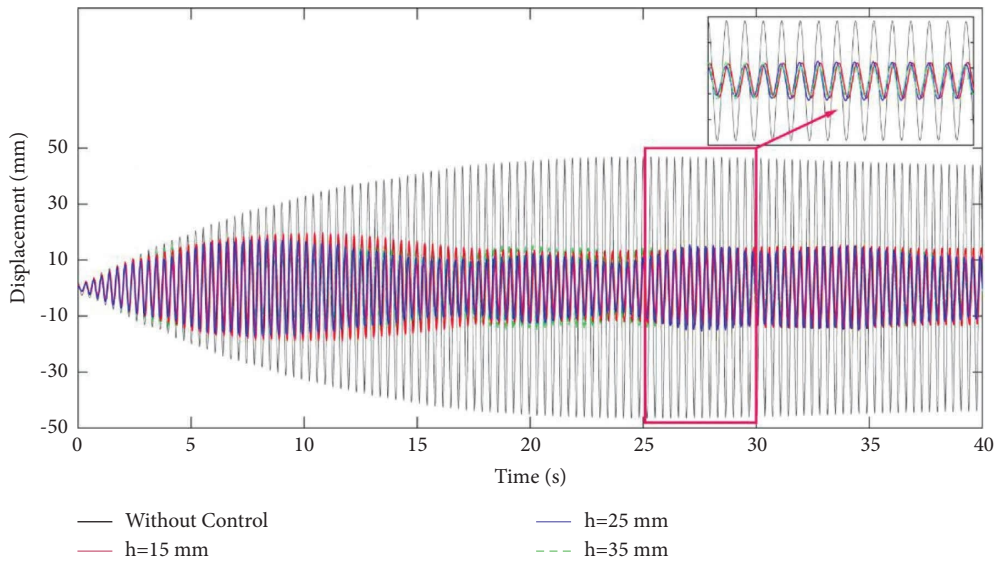

(a)

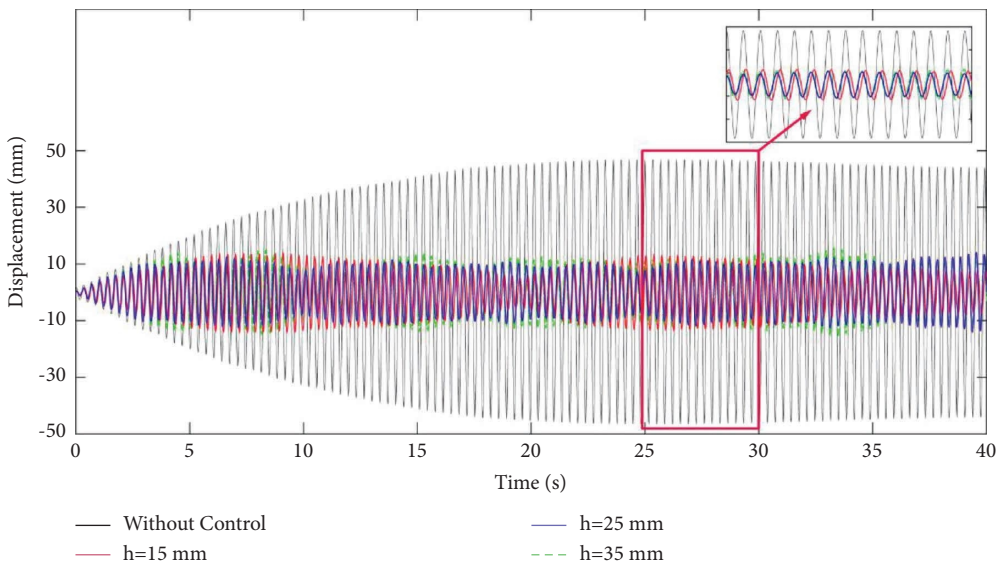

(b)

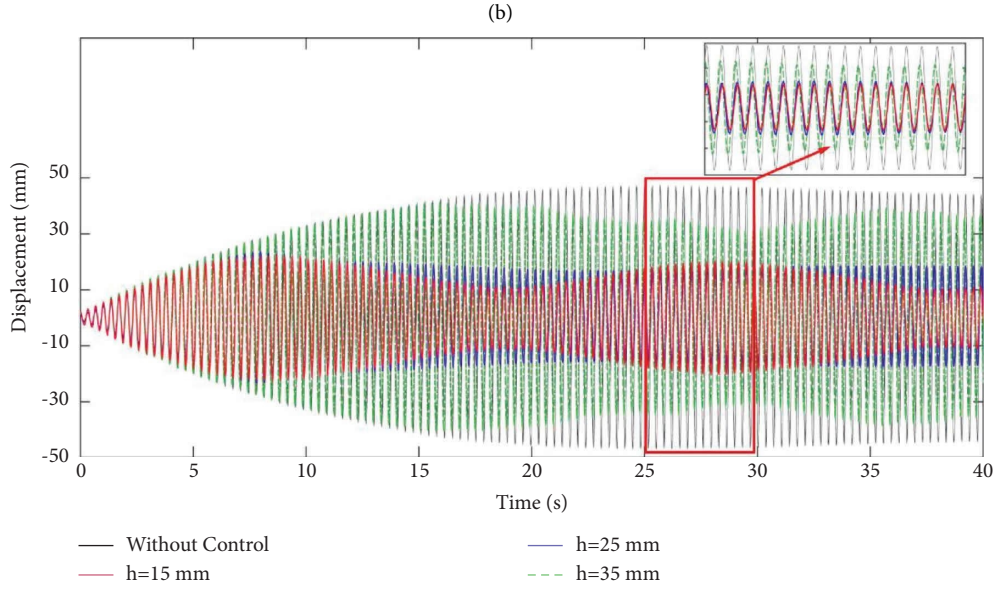

(c)

Figure 8: Continued.

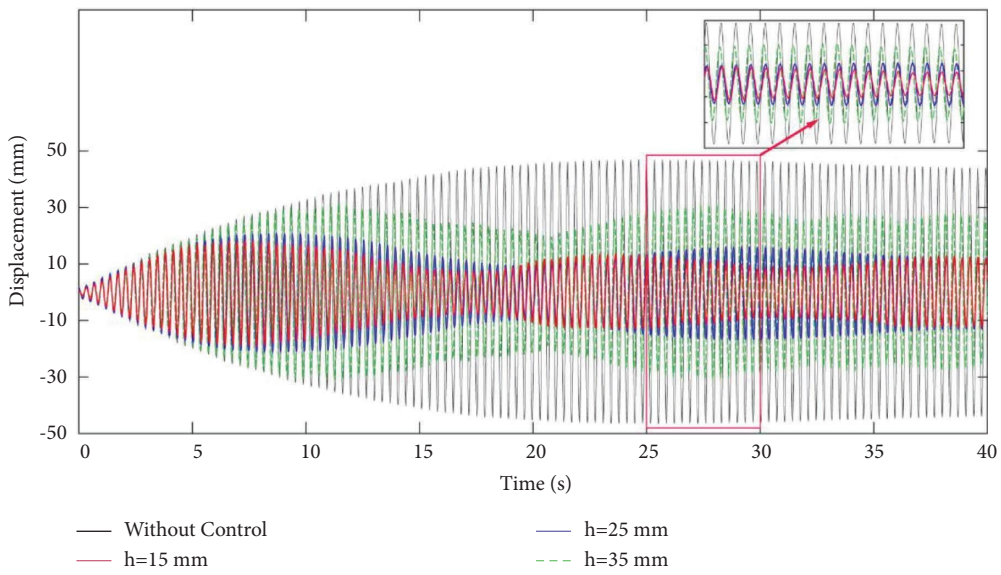

(d)

Figure 8: Time-history response of frame structure under different parameters: (a) $\delta = 0.2$ mm, $\mu = 1.37\%$, (b) $\delta = 0.2$ mm, $\mu = 2.21\%$, (c) $\delta = 0.25$ mm, $\mu = 1.37\%$, and (d) $\delta = 0.25$ mm, $\mu = 2.21\%$.

Table 5: Reduction of the peak displacement.

Arch height	$\delta = 0.2$ mm						$\delta = 0.25$ mm					
	$\mu = 1.37\%$			$\mu = 2.21\%$			$\mu = 1.37\%$			$\mu = 2.21\%$		
	w/o ctrl (mm)	w ctrl (mm)	Reduction ratiox (%)	w/o ctrl (mm)	w ctrl (mm)	Reduction ratio (%)	w/o ctrl (mm)	w ctrl (mm)	Reduction ratio (%)	w/o ctrl (mm)	w ctrl (mm)	Reduction ratio (%)
$h = 15$ mm	46.87	19.71	57.95	46.87	13.70	70.77	46.87	22.21	52.61	46.87	30.55	34.82
$h = 25$ mm	46.87	17.43	62.81	46.87	14.05	70.02	46.87	25.37	45.87	46.87	29.21	37.68
$h = 35$ mm	46.87	15.28	67.40	46.87	15.58	66.76	46.87	24.38	47.80	46.87	31.47	32.86

utilizing the NSBD, which not only mitigates vibrations an overall wide frequency range but also shifted the natural frequency far from the dominant frequency. Figure 8 illustrates the time-history response of frame structure with different parameters, and all detailed results are compared in Table 5.

Table 5 shows that the maximum attenuation of the peak displacement reached up to 70.77%. Among the different tested configurations, the damping effect is best when the thickness of NSBD is 0.2 mm. An explanation is that when the thickness of the NSBD is large, a larger driving force is needed to initiate the snap-through motion between the two equilibrium positions of the NSBD. Therefore, under the same external excitation, NSBD with a lower thickness is more prone to snap-through motion, which improves vibration attenuation. This improvement can be seen in Figure 7(a) vs Figure 7(c) and Figure 7(b) vs Figure 7(d). For the same beam thickness, the difference in arching height leads to significant differences in kinetic energy consumed when snap-through occurs. In these experiments, NSBD with a large arch height has a larger displacement time history, which indicates that the vibration mitigation effect is also more obvious, as shown in Figures 7(a) and 7(b), the same in Figures 7(c) and 7(d). The attenuating effect of NSBD on the frame structure is more intuitively derived from its displacement time history, as shown in Figure 8, and its experimental regulation is similar to that in Figure 7.

5.2. Control Effectiveness under Earthquake Excitation. The values of the parameters for the NSBD are selected by the vibration suppression effect of the NSBD under sinusoidal excitation in the shake table tests. It is noted from Figures 7(a) and 7(b) that the vibration suppression effect of the NSBD is better when its mass ratio is 2.21%. As shown in Figures 7(a) and 7(c), the vibration suppression effect of the NSBD is better when its thickness and height are 0.2 mm and 35 mm, respectively. The first set of tests uses six earthquake records selected according to Site classification I. To investigate the NSBD effectiveness with other site classes, four other earthquake records are selected according to Site classification II. The details of the selected earthquake excitations are listed in Table 4.

Figure 9 shows the displacement time histories of the frame structure (with and without optimized NSBD) during different earthquake excitations. The displacements of the

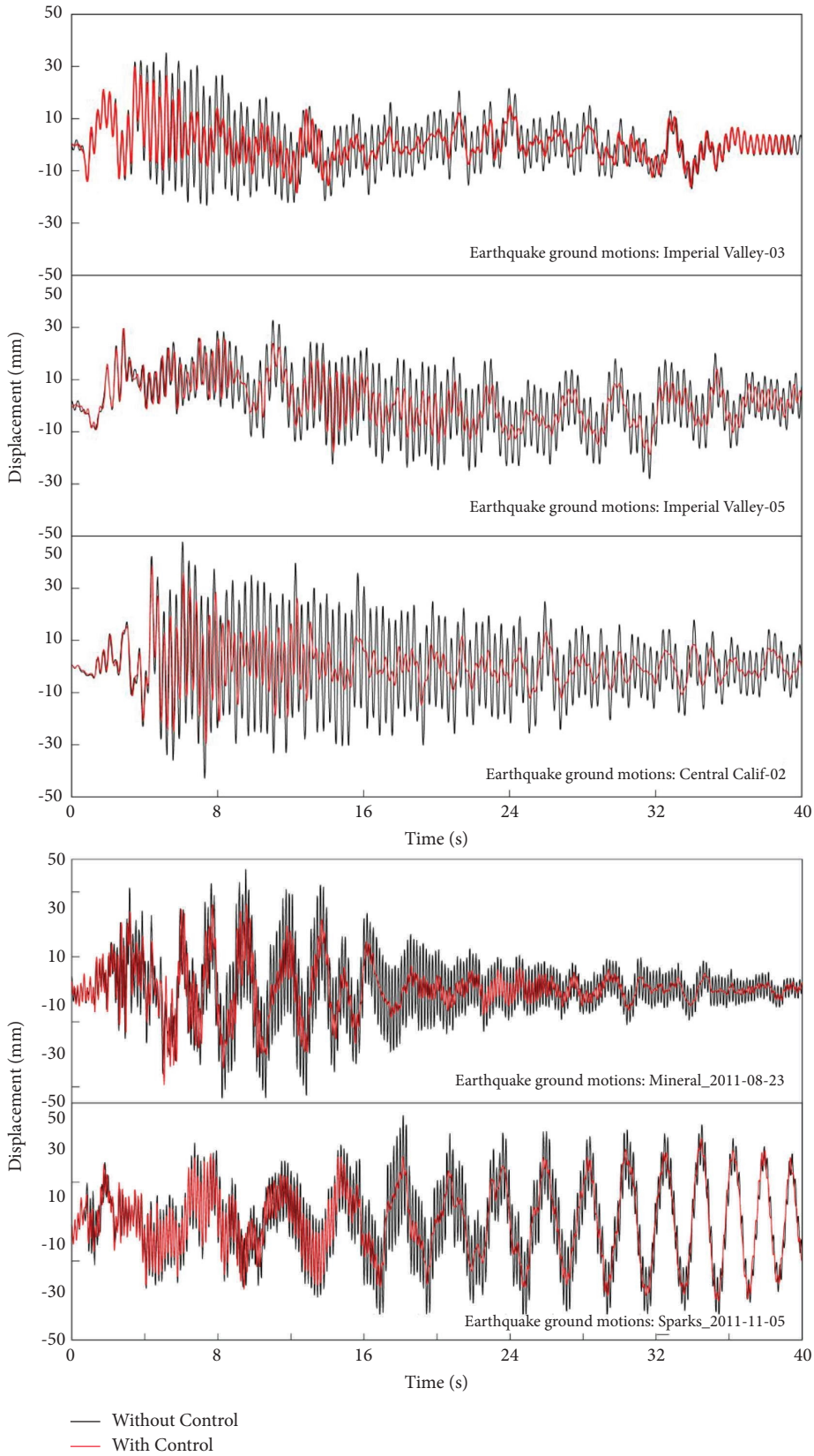

Figure 9: Time-history response of frame structure under different earthquake excitations: (a) Imperial Valley-03; (b) Imperial Valley-05; (c) Central Calif-02; (d) Mineral_2011-08-23; (e) Sparks_2011-11-05.

Table 6: Vibration reduction ratio of NSBD to frame structure under different earthquake excitations.

Earthquake excitations	P (%)	S_{rms} (%)
Imperial Valley-03	25.12	31.39
Southern Calif	26.83	26.79
Imperial Valley-05	26.89	25.89
Central Calif-02	25.14	45.03
Hollister-01	32.80	36.34
San Fernando	26.77	29.82
Guy_2010-10-15-HHE	24.58	40.50
Guy_2010-10-15-HHN	44.63	24.58
Mineral_2011-08-23	28.88	25.17
Sparks_2011-11-05	39.21	11.25

frame structure are generally reduced when the NSBD is installed. The peak vibration reduction ratio (P) and RMS vibration reduction ratio are both dependent on seismic motions, demonstrating that NSBD can improve the structure's resilience against hazardous earthquake ground motion. The peak vibration reduction ratio and RMS vibration reduction ratio can be obtained by equations (22) and (23), compared in Table 6. Table 6 shows that the peak damping ratio and average damping ratio can be attenuated respectively by up to 44.63% and 45.03%, demonstrating that the NSBD effectively suppresses the action of earthquake ground motion on the frame structure.

$$P = \frac{a_{\max 1}}{a_{\max 2}}, \tag{22}$$

where P refers to the peak vibration reduction ratio (%), $a_{\max 1}$ refers to the maximum displacement amplitude of the structure during the earthquake excitation when the NSBD is installed (mm), $a_{\max 2}$ refers to the maximum displacement amplitude of the structure during the earthquake excitation (mm).

$$S_{rms} = \frac{\sqrt{1/N \sum_{i=1}^{n} a_{1i}^2} = \sqrt{a_{11}^2 + a_{12}^2 + \cdots + a_{1n}^2/N}}{\sqrt{1/N \sum_{i=1}^{n} a_{2i}^2} = \sqrt{a_{21}^2 + a_{22}^2 + \cdots + a_{2n}^2/N}}, \tag{23}$$

where S_{rms} refers to RMS vibration reduction ratio (%), N refers to total time intervals, a_{1i} refers to the displacement of the structure during the earthquake excitation at per time interval when the NSBD is installed (mm), and a_{2i} refers to the displacement of the structure during the earthquake excitation at per time interval (mm).

In summary, the experimental results show that the proposed NSBD has an excellent vibration mitigation effect on the frame structure under both sinusoidal excitation and earthquake excitations.

6. Conclusions

The negative stiffness bistable damper (NSBD) is currently proposed to dampen the vibration response of the frame structure. The constitutive equation of the NSBD is derived to analyze the effects of stiffness ratio, arch-span ratio, and damping ratio on its restoring capabilities. To verify the vibration suppression performance of the NSBD, shaking table tests of a frame structure are conducted under different sinusoidal and seismic excitations with and without an NSBD. The results reveal that the NSBD can effectively restrain the displacements of the structure. In addition, the buckling beam cannot have significant deflection to allow it to vibrate between two equilibrium positions, meaning that the beam must remain in its elastic range for the NSBD to be effective. The main findings in the present study are summarized as follows:

The proposed damper can greatly mitigate the peak displacement of the frame structure at the dominant frequency and has a wide damping bandwidth. Furthermore, the control effectiveness of the NSBD is robust against a range of sinusoidal and seismic excitations, demonstrating that the NSBD can strengthen structural security against hazardous seismic events.

This paper only explored the attenuating effect of NSBD on a single-story frame structure experimentally. Future works will be undertaken to perform related analytical and numerical research. Furthermore, the vibration control of structures using the NSBD in actual engineering will be further studied and improved in future work.

Data Availability

The data used to support the findings of this study are included in the article.

Conflicts of Interest

The authors declare that they have no conflicts of interest.

References

[1] J. T. P. Yao, "Concept of structural control," *Journal of the Structural Division*, vol. 98, no. 7, pp. 1567–1574, 1972.

[2] D. R. Johnson, R. L. Harne, and K. W. Wang, "A disturbance cancellation perspective on vibration control using a bistable snap-through attachment," *Journal of Vibration and Acoustics*, vol. 136, no. 3, Article ID 031006, 2014.

[3] A. De Luca and L. G. Guidi, "State of art in the worldwide evolution of base isolation design," *Soil Dynamics and Earthquake Engineering*, vol. 125, Article ID 105722, 2019.

[4] D. Kim, "Effect of frequency characteristics of ground motion on response of tuned mass damper controlled inelastic concrete frame," *Buildings*, vol. 11, no. 74, pp. 1–19, 2021.

[5] S. Zhang, Y. Hu, C. Zhang, S. Li, and P. Tan, "Performance-based compositive passive control analysis of multi-tower building with chassis: optimization of Kelvin-Voigt dampers," *Buildings*, vol. 12, no. 2, p. 137, 2022.

[6] Gregorski and Tim, "Akashi Kaikyo bridge," *Roads and Bridges*, vol. 36, no. 8, 1998.

[7] X. D. Tang and L. Zuo, "Passive, active and semi-active series tuned mass dampers," in *Proceedings of the Conference on Active and Passive Smart Structures and Integrated Systems*, San Diego, CA, USA, March 2010.

[8] X. L. Lu and J. R. Chen, "Mitigation of wind-induced response of Shanghai Center Tower by tuned mass damper," *The Structural Design of Tall and Special Buildings*, vol. 20, no. 4, pp. 435–452, 2011.

[9] X. Liu, Y. Yang, Y. Sun, Y. Zhong, and L. Zhou, "Inerter location-based vibration suppression study of a transmission

line equipped with tuned-mass-damper-inerter (TMDI) under harmonic excitation," *Buildings*, vol. 12, no. 5, p. 657, 2022.

[10] J. Yu, Z. Li, Z. Zhang, W. Zhao, Z. Niu, and J. Cheng, "Vibration test and control of factory a building under excitation of multiple vibrating screens," *Buildings*, vol. 12, no. 5, p. 607, 2022.

[11] J. Zhang, Y. Zhu, Z. Li, and J. Tu, "Research on optimal placement of actuators of high-rise buildings considering the influence of seismic excitation on structural modes," *Buildings*, vol. 12, no. 1, p. 8, 2021.

[12] W. G. Molyneux, *Supports for Vibration isolation*, Aeronautical Research Council, Great Britain,UK, 1957.

[13] A. Carrella, M. J. Brennan, and T. P. Waters, "Optimization of a quasi-zero-stiffness isolator," *Journal of Mechanical Science and Technology*, vol. 21, no. 6, pp. 946–949, 2007.

[14] C. Cheng, S. Li, W. Yong, and X. Jiang, "On the analysis of a piecewise nonlinearlinear vibration isolator with highstatic-lowdynamic-stiffness under base excitation," *Journal of Vibroengineering*, vol. 17, no. 7, pp. 3453–3470, 2015.

[15] T. H. Wu and C. C. Lan, "A wide-range variable stiffness mechanism for semi-active vibration systems," *Journal of Sound and Vibration*, vol. 363, pp. 18–32, 2016.

[16] X. Liu, X. Huang, and H. Hua, "On the characteristics of a quasi-zero stiffness isolator using Euler buckled beam as negative stiffness corrector," *Journal of Sound and Vibration*, vol. 332, no. 14, pp. 3359–3376, 2013.

[17] H. Mori, T. Waters, N. Saotome, T. Nagamine, and Y. Sato, "The effect of beam inclination on the performance of a passive vibration isolator using buckled beams," *Journal of Physics: Conference Series*, vol. 744, no. 1, Article ID 012229, 2016.

[18] R. Ravaud, G. Lemarquand, S. Babic, V. Lemarquand, and C. Akyel, "Cylindrical magnets and coils: fields, forces, and inductances," *IEEE Transactions on Magnetics*, vol. 46, no. 9, pp. 3585–3590, 2010.

[19] J. Zhou, Q. Xiao, D. Xu, H. Ouyang, and Y. Li, "A novel quasi-zero-stiffness strut and its applications in six-degree-of-freedom vibration isolation platform," *Journal of Sound and Vibration*, vol. 394, pp. 59–74, 2017.

[20] D. Xu, Q. Yu, J. Zhou, and S. R. Bishop, "Theoretical and experimental analyses of a nonlinear magnetic vibration isolator with quasi-zero-stiffness characteristic," *Journal of Sound and Vibration*, vol. 332, no. 14, pp. 3377–3389, 2013.

[21] J. Zhou, X. Wang, D. Xu, and S. Bishop, "Nonlinear dynamic characteristics of a quasi-zero stiffness vibration isolator with cam–roller–spring mechanisms," *Journal of Sound and Vibration*, vol. 346, pp. 53–69, 2015.

[22] C. Cheng, S. Li, Y. Wang, and X. Jiang, "On the analysis of a high-static-low-dynamic stiffness vibration isolator with time-delayed cubic displacement feedback," *Journal of Sound and Vibration*, vol. 378, pp. 76–91, 2016.

[23] C. Ren, D. Yang, and H. Qin, "Mechanical performance of multidirectional buckling-based negative stiffness metamaterials: an analytical and numerical study," *Materials*, vol. 11, no. 7, p. 1078, 2018.

[24] B. Haghpanah, A. Shirazi, L. Salari-Sharif, A. Guell Izard, and L. Valdevit, "Elastic architected materials with extreme damping capacity," *Extreme Mechanics Letters*, vol. 17, pp. 56–61, 2017.

[25] L. N. Virgin, S. T. Santillan, and R. H. Plaut, "Vibration isolation using extreme geometric nonlinearity," *Journal of Sound and Vibration*, vol. 315, no. 3, pp. 721–731, 2008.

[26] X. Shi and S. Y. Zhu, "Magnetic negative stiffness dampers," *Smart Materials and Structures*, vol. 24, no. 7, Article ID 072002, 2015.

[27] J. Zhou, D. Xu, and S. Bishop, "A torsion quasi-zero stiffness vibration isolator," *Journal of Sound and Vibration*, vol. 338, pp. 121–133, 2015.

[28] C. Xiang, H. Li, and H. Liu, "A study on the damping characteristics of semi-active torsional damper with combined positive and negative stiffness in parallel," *Automotive Engineering*, vol. 37, no. 4, p. 430, 2015.

[29] P. Zhou, M. Liu, and H. Li, "A passive negative stiffness damper in series with a flexible support: theoretical and experimental study," *Structural Control and Health Monitoring*, vol. 27, no. 9, Article ID e2594, 2020.

[30] H. Li, Y. Yu, J. Li, Y. Li, and M. Askari, "Multi-objective optimisation for improving the seismic protection performance of a multi-storey adaptive negative stiffness system based on modified NSGA-II with DCD," *Journal of Building Engineering*, vol. 43, Article ID 103145, 2021.

[31] W. Guo, L. Guo, Z. Zhai, and S. Li, "Seismic performance assessment of a super high-rise twin-tower structure connected with rotational friction negative stiffness damper and lead rubber bearing," *Soil Dynamics and Earthquake Engineering*, vol. 152, Article ID 107039, 2022.

[32] H. Li, J. Li, and K. Bi, "A quasi-active negative stiffness damper for structural vibration control under earthquakes," *Mechanical Systems and Signal Processing*, vol. 173, Article ID 109071, 2022.

[33] Y. Wang, Q. Chen, Z. Zhao, H. Qiang, B. Liu, and X. Wang, "Multi-location seismic isolation approach and design for underground structures employing the negative-stiffness amplification system," *Tunnelling and Underground Space Technology*, vol. 122, Article ID 104395, 2022.

[34] Q. Liang and L. Li, "Dynamic performance of time-domain piecewise linear stiffness system," *Journal of Engineering Mechanics*, vol. 147, no. 7, p. 2021, 2021.

[35] M. Wang, S. Nagarajaiah, and F.-F. Sun, "Optimal design of supplemental negative stiffness damped outrigger system for high-rise buildings resisting multi-hazard of winds and earthquakes," *Journal of Wind Engineering and Industrial Aerodynamics*, vol. 218, Article ID 104761, 2021.

[36] X. Shi, X. Guan, W. Shen, and L. Xing, "A control strategy using negative stiffness and semi-active viscous damping for fully tracking active control force for bridge cables: principles and simulations," *Structural Control and Health Monitoring*, vol. 29, Article ID e2989, 2022.

[37] M. Wang, Y.-W. Li, S. Nagarajaiah, and Y. Xiang, "Effectiveness and robustness of braced-damper systems with adaptive negative stiffness devices in yielding structures," *Earthquake Engineering & Structural Dynamics*, vol. 51, Article ID eqe.3693, 2022.

[38] Q. H. Liu, J. Y. Cao, F. Y. Hu, D. Li, X. Jing, and Z. Hou, "Parameter identification of nonlinear bistable piezoelectric structures by two-stage subspace method," *Nonlinear Dynamics*, vol. 105, no. 3, pp. 2157–2172, 2021.

[39] M. Lin and Y.-M. Huang, "Stochastic resonance control based on vibration resonance," *Acta Physica Sinica*, vol. 56, no. 11, pp. 6173–6177, 2007.

[40] D. R. Johnson, R. L. Harne, K. W. Wang, and Asme, "On vibration control using a bistableI snap through absorber from a force balance perepective," in *Proceedings of the ASME International Design Engineering Technical Conferences and Computers and Information in Engineering Conference (IDETC/CIE)*, Portland, OR, August 2013.

[41] S. Farhangdoust, P. Eghbali, and D. Younesian, "Bistable tuned mass damper for suppressing the vortex induced vibrations in suspension bridges," *Earthquakes and Structures*, vol. 18, no. 3, pp. 313–320, 2020.

[42] Y. Xia, M. Ruzzene, and A. Erturk, "Bistable attachments for wideband nonlinear vibration attenuation in a metamaterial beam," *Nonlinear Dynamics*, vol. 102, no. 3, pp. 1285–1296, 2020.

[43] J. Zhao, K. Cheng, R. Gao, M. Huang, and P.-B. Liu, "Snap-through bifurcation analysis of compliant bistable structures," *Journal of Mechanical Engineering*, vol. 55, no. 5, pp. 74–81, 2019.

[44] E. C. Liu, X. Fang, J. H. Wen, and D. L. Yu, "1/2 sub-harmonic resonance in bistable structure and its effect on vibration isolation characteristics," *Acta Physica Sinica*, vol. 69, no. 6, Article ID 064301, 2020.

[45] X. Zhang, *Design of Automobile Energy Absorbing Structure Based on Bistable Variable Stiffness characteristics*, Dalian University of Technology, Dalian, China, 2020.

[46] B. Yan, H. Ma, L. Zhang, W. Zheng, K. Wang, and C. Wu, "A bistable vibration isolator with nonlinear electromagnetic shunt damping," *Mechanical Systems and Signal Processing*, vol. 136, Article ID 106504, 2020.

[47] B. Yan, P. Ling, Y. Zhou, C. Wu, and W. Zhang, "Shock isolation characteristics of a bistable vibration isolator with tunable magnetic controlled stiffness," *Journal of Vibration and Acoustics*, vol. 144, no. 2, 2022.

[48] Z. Zhang, F. Shi, C. Yang, and Z.-D. Xu, "Quasi-zero stiffness isolator based on bistable structures with variable cross-section," *Journal of Low Frequency Noise, Vibration and Active Control*, vol. 41, no. 1, pp. 405–416, 2022.

[49] K. Yang, W. Tong, L. Lin, D. Yurchenko, and J Wang, "Active vibration isolation performance of the bistable nonlinear electromagnetic actuator with the elastic boundary," *Journal of Sound and Vibration*, vol. 520, Article ID 116588, 2022.

[50] J. Qiu, J. H. Lang, A. H. Slocum, and A. C. Weber, "A bulk-micromachined bistable relay with U-Shaped thermal actuators," *Journal of Microelectromechanical Systems*, vol. 14, no. 5, pp. 1099–1109, 2005.

[51] China Architecture and Building Press, "Code for Secismic Design of Buildings; GB50011-2010," China Architecture and Building Press, Beijing, China, 2016.